JACS
JOURNAL OF THE AMERICAN CHEMICAL SOCIETY
Article
pubs.acs.org/JACS

Fluorescence Coupling for Direct Imaging of Electrocatalytic Heterogeneity

Joshua P. Guerrette, Stephen J. Percival, and Bo Zhang*

Department of Chemistry, University of Washington, Seattle, Washington 98195-1700, United States

Supporting Information

ABSTRACT: Here we report the use of fluorescence microscopy and closed bipolar electrodes to reveal electrochemical and electrocatalytic activity on large electrochemical arrays. We demonstrate fluorescence-enabled electrochemical microscopy (FEEM) as a new electrochemical approach for imaging transient and heterogeneous electrochemical processes. This method uses a bipolar electrode mechanism to directly couple a conventional oxidation reaction, e.g., the oxidation of ferrocene, to a special fluorogenic reduction reaction. The generation of the fluorescent product on the cathodic pole enables one to directly monitor an electrochemical process with optical microscopy. We demonstrate the use of this method on a large electrochemical array containing thousands or more parallel bipolar microelectrodes to enable spatially and temporally resolved electrochemical imaging. We first image molecular transport of a redox analyte in solution using an array containing roughly 1000 carbon fiber ultramicroelectrodes. We then carry out a simple electrocatalysis experiment to show how FEEM can be used for electrocatalyst screening. This new method could prove useful for imaging transient electrochemical events, such as fast exocytosis events on single and networks of neurons, and for parallel, high-throughput screening of new electrocatalysts.

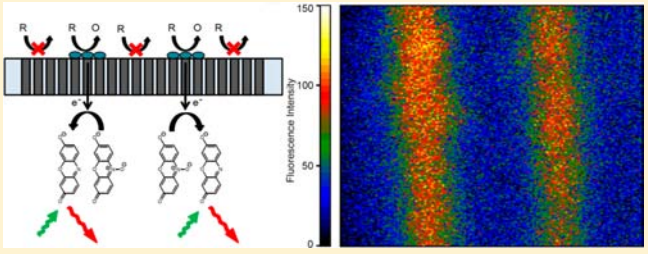

INTRODUCTION

The ability to spatially and temporally resolve electrochemical processes has become increasingly important for many investigations in the past several decades, particularly for electrocatalysis studies[1] and studies involving heterogeneous electrode surfaces[2] and biological redox processes.[3] Among the most widely applied electrochemical imaging methods is scanning electrochemical microscopy (SECM), which relies on the rastering of an ultramicroelectrode over a substrate of interest to obtain topographical or electrochemical information.[4,5] SECM has proven to be extremely valuable for applications, such as mapping a catalytic surface,[6,7] studying molecular transport at localized domains,[8−11] and imaging single biological cells.[12,13] In addition to the stand alone technique, SECM has been combined with other imaging techniques, such as atomic force microscopy (AFM)[14] and scanning ion-conductance microscopy (SICM).[15−17] Despite these outstanding properties, it is necessary, however, with SECM to make a compromise between image spatial resolution, scan time, and size of working area. Several attempts have been reported to overcome this limitation, most notably by Girault and co-workers who have used flexible linear microelectrode arrays to minimize the total scan duration.[18,19] However, if faster temporal information is desired for transient or short-lived processes, a scanning technique will not suffice.

Tao and co-workers have recently introduced an elegant electrochemical imaging method, which utilizes surface plasmon resonance (SPR) to detect local changes in current density[20,21] or electrochemical impedance[22,23] and to perform square wave voltammetry[24] at thin film gold electrodes. Their method can obtain data comparable to a conventional voltammetric response over various regions of an electrode with excellent sensitivity for small redox species, such as $Ru(NH_3)_6^{3+}$ or TNT. However, this method requires the use of a thin-film gold electrode, which may limit its application in certain processes. Additionally, certain redox processes involving larger electroactive molecules may likely involve relatively little change in the index of refraction and thus a weak signal. Another challenge with this technique may be the deconvolution of local SPR changes due to heterogeneity of the electrochemical current from irregularities due to electrode surface functionalizations themselves.

To address the aforementioned challenges it would be desirable to use an array of thousands or more individually and simultaneously addressable microelectrodes. This, however, presents several major challenges, both in the array fabrication and the complex and costly electronics/data acquisition requirements for monitoring such an extreme number of channels. The Ewing group has extended the traditional limit to the numbers and size of microelectrode arrays for electrochemical analysis[25,26] including a recent report using an array containing 15 ultramicroelectrodes.[27] This has allowed for the direct imaging of transient exocytosis events from single cells.

Received: October 26, 2012
Published: December 17, 2012

   dx.doi.org/10.1021/ja310401b | J. Am. Chem. Soc. 2013, 135, 855−861

In order to significantly increase the number of simultaneously addressable electrodes and to spatially resolve smaller features, an alternative method for addressing individual microelectrodes and monitoring their current is necessary.

Here we report a new electrochemical approach, called fluorescence-enabled electrochemical microscopy (FEEM), to locally monitor electrochemical current on large electrochemical arrays. This method couples a fluorogenic redox reaction to the redox reaction of interest so that one can use fluorescence microscopy to examine a conventional faradaic reaction on individual microelectrodes. Extending this strategy on a closed bipolar electrochemical array allows one to simultaneously monitor thousands of electrodes. Figure 1a illustrates the basic principles of FEEM. At the core of the setup is a closed bipolar electrode,[28,29] which along with its surrounding insulative substrate completely separates the two solution compartments. One solution compartment contains an oxidizable redox analyte (**R**), while the other contains a buffered solution of resazurin (**S**). No direct electrical contact is made to the bipolar electrode from the external circuit thus simplifying the electrical setup. Instead, a small bias voltage is applied to two electrodes to couple the redox reactions on the bipolar electrode. The oxidation of **R** to **O** at the anodic pole is coupled to the two-electron, two-proton fluorogenic reduction of resazurin (Figure 1b). Optical monitoring of the fluorescent product of this reaction, resorufin (**P**), provides a convenient and sensitive way to measure the electrochemical signal of the analyte.

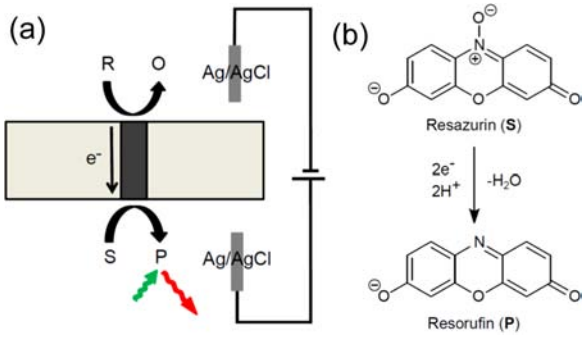

Figure 1. (a) A schematic illustrating the basic principle of FEEM and (b) the fluorogenic reduction of resazurin.

The use of fluorescence microscopy to study electrochemical processes is itself not a new concept. Fluorescence-voltage single molecule spectroscopy (F-V/SMS)[30] and single-molecule spectroelectrochemistry (SMS-EC), developed by Barbara and Bard and their co-workers[31,32] has led to much related work for the study of electron transfer kinetics[33] and electrocatalytic reduction[34,35] of single organic dyes. While all of these studies demonstrate applications of fluorescence-based electrochemical detection, their usefulness is strictly limited to investigations into the properties of a limited number of redox active fluorophores or special fluorogenic redox reactions. FEEM instead relies on the fluorogenic reaction only to report the rate of electrochemical processes involving redox species with no inherent fluorescence of their own. This makes possible the broad application of FEEM to study nearly any redox active species.

A unique advantage of this method is the ability to individually and simultaneously address a large number of parallel microelectrodes (e.g., $>10^4$) and optically monitor their faradaic response. The absence of a direct connection and the conversion of an electrochemical current signal to a fluorescence signal allow for the use of a large array of parallel bipolar electrodes. This provides a new means to spatially and temporally resolve electrochemical processes. In this report we first provide the initial demonstration of FEEM using two series-coupled microelectrodes. Next, electrochemical arrays containing thousands of ultramicroelectrodes are used to image redox species discharged from a glass micropipet. Finally, due to the growing interest in electrocatalyst screening,[36,37] we demonstrate the use of FEEM to map catalytically active hot spots on a carbon fiber electrode array, which was selectively patterned and modified with Pt. Although this simple demonstration here uses only two materials, it can be easily scaled up for high-throughput, parallel, multicomponent screening of electrocatalysts.

EXPERIMENTAL SECTION

Chemicals and Materials. Ferrocene (Fc, Fluka Analytical), ferrocenemethanol (FcMeOH, Aldrich), hydrogen peroxide (30%, J.T. Baker), tetra-*n*-butylammonium hexafluorophosphate ($TBAPF_6$, Aldrich), potassium chloride (J.T. Baker), sodium sulfate (Fisher Chemicals), sodium hydroxide (J.T. Baker), monosodium phosphate (Fisher), disodium phosphate (J.T. Baker), platinum(IV) chloride (Aldrich), sulfuric acid (EMD Chemicals), and reagent grade acetonitrile (MeCN, Aldrich) were all used without further purification. Resazurin sodium salt (Aldrich) containing resorufin in small quantities was purified using previously established procedures.[38] A Barnstead Nanopure water purification system was used to provide >18 MΩ·cm deionized water for all aqueous solutions.

Fabrication of Bipolar CF Electrode Arrays and Pt Deposition. Carbon pultrusion rods (OD 0.280−4 mm) consisting of hundreds or thousands of individual 6 μm-diameter carbon fibers within an insulative epoxy binder were obtained from DPP Pultrusion through the distributor A2Z Corp. Sections of the rods were further sealed in Epo-Tek 301epoxy (Epoxy Technologies, Inc.) to further increase rigidity and provide additional isolation between both ends of the rods. Thin cross sections of the resulting carbon fiber/epoxy rods were cut and then polished to the desired final thickness from ∼0.1 to 4 mm. CF arrays to be selectively patterned with Pt were first patterned with photoresist. Samples were spin coated with adhesion promoter (Micro Prime MP-P20 (20% hexamethyldisilazane (HMDS), 80% propylene glycol monomethyl-ether acetate (PGMEA)), then with AZ1512 photoresist (AZ Corporation). Patterning was accomplished using a chromium-on-glass UV mask and a Newport UV Flood Exposure System with a 500 W Hg lamp followed by developing to expose the selected carbon fibers (AZ351 developer AZ Corporation, diluted 1:5 developer:DI H_2O). Pt was deposited on exposed carbon fibers using a solution of 1 mM $PtCl_4$ and 0.5 M H_2SO_4 in a bipolar deposition configuration. To provide electron transfer at the anodic poles of the CF array a solution of 2 mM FcMeOH in 0.1 M KCl was used and a potential pulse of −1.6 V for 200 ms followed by a resting potential of 0 V for 800 ms. The voltage was applied to two Ag/AgCl QREs for a total of 5 min.

FEEM Apparatus Setup. An Olympus IX70 inverted microscope equipped with an IX-FLA inverted reflected light fluorescence observation attachment was used for all fluorescence experiments. Illumination was provided using an Olympus U-ULS100HG 100 W mercury burner. A filter set consisting of a HQ535/50 excitation filter, a Q565lp dichroic mirror, and a HQ610/75 emission filter was used. Video/images were recorded using an Andor iXon+EMCCD camera cooled to −80 °C and a Dell PC equipped with Andor SOLIS software. Electric potential was applied to two AgCl-coated Ag wire quasireference electrodes through a Chem-Clamp potentiostat (Dagan) connected to an EG&G 175 programmer. Voltammetric response was recorded using a PCI-6251 (National Instruments) card on a Dell PC using in-house LabView 8.5 software (National

dx.doi.org/10.1021/ja310401b | J. Am. Chem. Soc. 2013, 135, 855−861

Instruments). A scan rate of 200 mV/s was used for all potential sweep experiments unless noted otherwise.

Video Acquisition and Processing. Andor SOLIS software was used for all video/image recording and postprocessing. Video was recorded at a frame rate of 19.81 Hz for the experiments shown in Figure 4 and 33.887 Hz for all other experiments. A preamplifier gain setting of 5.1 was used. Time derivative of fluorescent intensity is presented as a moving average for Figure 2b (n = 30) and Figure 6 (n = 10) to smooth short-term fluctuations in fluorescent signal.

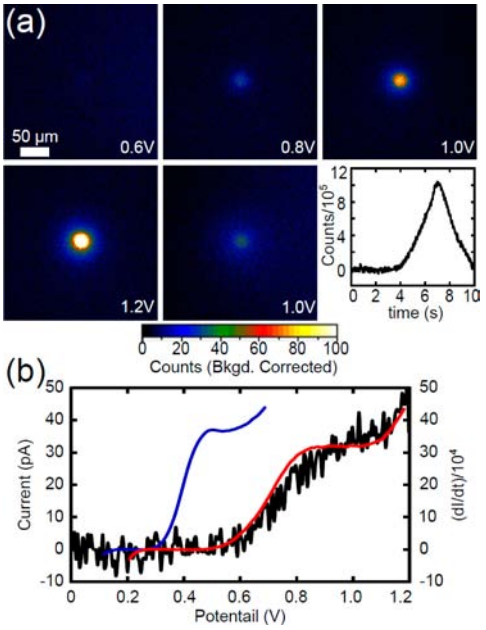

Figure 2. (a) A series of fluorescence images over the course of a potential sweep experiment (0−1.4 V, 200 mV/s) for the detection of 2.5 μM Fc using 50 μM resazurin in a 50 mM phosphate buffer pH = 7.4. The last panel shows the total fluorescence counts plotted as a function of time during the voltage sweep. (b) Voltammetric response of a 25 μm Au disk electrode in 2.5 μM Fc (blue curve), the response when the same electrode is connected in series to another 25 μm Au disk electrode in 50 μM resazurin (red curve) and the time derivative of the fluorescence intensity (black trace) for the experiment shown in (a) as a function of potential from 0 to 1.2 V.

Scanning Electron Microscopy. Scanning Electron Microscopy (SEM) images were obtained using a field-emission electron microscope (FEI Sirion). Samples were sputter coated with a thin layer (2−3 nm) of Au/Pd prior to imaging.

RESULTS AND DISCUSSION

Fluorescence Coupling on a Closed Bipolar Electrode.

Here, we first use a simple closed bipolar electrode to demonstrate electrochemical coupling between the oxidation of ferrocene and the reduction of resazurin. Two 25 μm diameter Au disk electrodes (SEM of the electrode surface shown in Figure SI1) were connected in series to create a closed bipolar electrode, as shown in Figure SI2. The anodic pole was placed in an acetonitrile solution containing 2.5 μM ferrocene and 0.1 M $TBAPF_6$, while the cathodic pole was placed in an aqueous solution containing 50 μM resazurin and 50 mM phosphate buffer (pH = 7.4). The solution surrounding the cathodic pole was illuminated (with a Hg lamp and a HQ535/50 excitation filter) to excite resorufin fluorescence. A triangular potential waveform 0−1.4 V was applied on the bipolar cell at a scan rate of 200 mV/s to oxidize ferrocene. This process was coupled to the reduction of resazurin to generate resorufin as a fluorescent product on the cathodic pole. Figure 2a shows five background corrected snapshots at selected voltages taken from a video recording a burst of fluorescence throughout the course of the potential sweep experiment. The sixth panel in Figure 2a is a plot of the fluorescence intensity versus time for the region over the electrode surface. The fluorescence signal seen here is the product of coupling the two electrochemical reactions, the oxidation of ferrocene and the fluorogenic reduction of resazurin, through the closed bipolar electrode.

For comparison Figure 2b shows the voltammetric responses of a 25 μm diameter Au disk electrode in 2.5 μM Fc in a conventional two-electrode cell (blue) and the corresponding closed bipolar configuration as used in the above fluorescent experiment (red). It can be seen here that the current−voltage response of the bipolar configuration is somewhat broader than the response from the conventional cell, and the curve is shifted to higher potentials. This change in wave slope is the result of coupling these two electrochemical processes and is not itself an indication of kinetic limitations.[39] Additionally, the position of the curve (i.e., the half-wave potential) can be approximated by taking the difference between formal potentials for the reactions at each of the two poles of the bipolar electrode. A more detailed discussion of the voltammetric response of closed bipolar electrodes can be found in our recent work.[28,39] The black curve shown in Figure 2b is the time derivative of the fluorescent intensity, dI/dt, at different applied potentials during the forward scan from 0 to 1.2 V. A nice correlation can be seen between the "fluorescence current" (black curve) and the corresponding electrochemical current (red curve). The total fluorescent count should be proportional to the total number of fluorescent resorufin molecules, which, by Faraday's law ($Q = nFN$), is proportional to the total charge passed through the bipolar electrode. As such, the time derivative of the fluorescence count, dI/dt, could generate a response linearly correlated to the faradaic current response. A more detailed explanation and derivation of the relationship between the Faradaic current and the time derivative of the fluorescence intensity are given in the Supporting Information (SI). Lei et al. have also recently shown the correlation between the derivative of fluorescence intensity and measured electrochemical current for the quasireversible oxidation of cresyl violet.[33] Here, due to the relatively low concentration of ferrocene, the oxidation reaction on the anodic pole limits the overall faradaic response of bipolar electrode, and the resulting "fluorescent voltammetric response" in Figure 2b is representative primarily of the oxidation of ferrocene. At short time intervals this relationship holds true, however, other factors, such as photobleaching, diffusion of fluorescent product resorufin and, at elevated potentials, further reduction of resorufin to the nonfluorescent dihydroresorufin,[34] may lead to a more convoluted signal at extended times. Quantification of the fluorescent response and its exact relationship to electrochemical current are an inherently difficult task. This would require consideration of the extinction coefficients and quantum efficiencies of both the fluorescent product and the redox active precursor, the detector efficiency as well as other less easily quantifiable factors, such as those discussed above. For this reason we believe that FEEM, in its present configuration, is more useful for measurements of relative electrochemical response. Additional controls and standards could be introduced into an experimental configuration to yield a more quantifiable result.

Figure 3 shows the results of several additional FEEM experiments for the oxidation of dopamine over the course of a

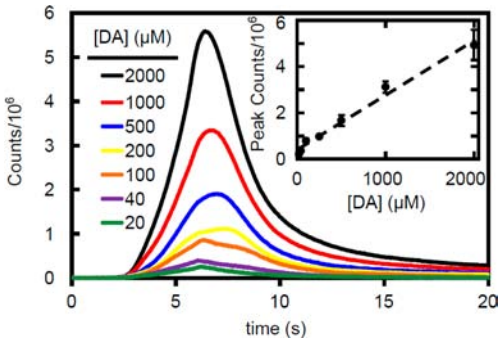

Figure 3. Fluorescence intensity for several FEEM experiments during a potential sweep (0.4 −1.6 V, 200 mV/s) for the oxidation of dopamine (DA) using two series coupled, 25 μm diameter Au disk electrodes and the concentration dependence of the peak fluorescence intensity (inset).

potential sweep. The oxidation of dopamine and the reduction of resazurin are both two-electron electrochemical processes. Thus, we anticipate that there is a 1:1 ratio between the total oxidized dopamine on the anodic pole and the generated resorufin on the cathodic pole. Indeed, here we see a linear correlation between peak fluorescence intensity and dopamine concentration. In this present experimental configuration, the limit of detection was ~1 μM, which corresponds to an oxidation limiting current of ~10 pA on the 25 μm diameter gold ultramicroelectrode.[40] However, other parameters including volume and concentration of the resazurin solution and method of fluorescence monitoring may be adjusted in order to increase sensitivity. A more systematic study is needed to better understand the relationship between fluorescence generation and electrochemical current including the possible use of other fluorogenic reporter reactions to improve sensitivity as well as to detect reducible analytes.

Fluorescence-Enabled Electrochemical Imaging. A unique advantage of this method is that it can be used on an array of ultramicroelectrodes to image dynamic and heterogeneous redox processes. We demonstrate this concept using a carbon-fiber ultramicroelectrodes array. Figure 4a illustrates a scheme of an experiment designed to electrochemically image redox species. Here we use this array to detect and image FcMeOH molecules as they are released from a glass micropipet. An SEM image of the microelectrode array is shown in Figure SI3. This array consisted of nearly 1000 parallel carbon fibers, each with a diameter of ~6 μm and a length of ~200 μm, insulated from each other by epoxy. A constant voltage of 800 mV was applied between the two Ag/AgCl driving electrodes in the anodic (top) and cathodic (bottom) solution compartments. The 3 μm inner diameter tip micropipet containing an aqueous solution of 2 mM FcMeOH with 0.1 M Na_2SO_4 was placed at the left most edge of the array adjacent to the anodic poles (top) and discharged for 5 s at 1 PSI. A burst of fluorescence was immediately observed at the corresponding location on the cathodic poles of the bipolar array. An image showing the initial burst of fluorescence is presented in the top left panel of Figure 4b and demonstrates the ability to spatially resolve transient presence of FcMeOH near the surface of the carbon electrodes. A series of six snapshots is presented in Figure 4b showing the growing

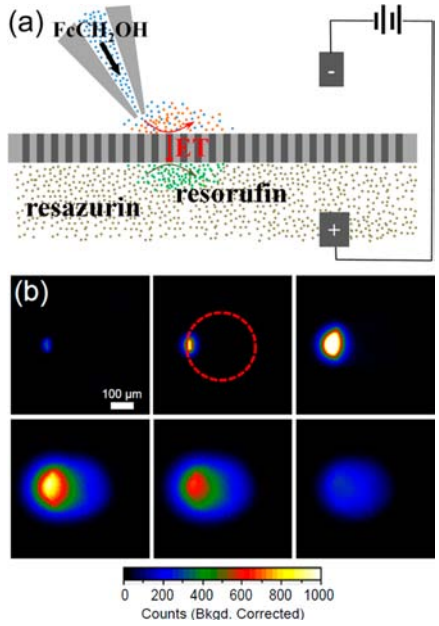

Figure 4. (a) Schematic diagram showing the setup to image release of FcMeOH from a glass micropipet with an array of carbon-fiber ultramicroelectrodes. The FcMeOH molecules are oxidized on the top surface of the carbon electrodes generating resorufin on the bottom surface of the carbon rods. (b) Fluorescence snapshots recorded from an experiment in which a solution of 2 mM FcMeOH with 0.1 M Na_2SO_4 was discharged from a 3 μm micropipet for 5 s at 1 PSI onto the left most side of a CF array with a total diameter of 300 μm.

fluorescent signal with time as more FcMeOH molecules are released from the pipet. The mass transport of FcMeOH at the anodic side of the array is visualized in this process. One drawback of this method, however, is the loss of spatial resolution due to diffusion of the fluorescent product along the surface of the microelectrode array. Figure SI4 shows the fluorescence intensities for select regions both to the right of the pipet tip location over the array and to the left of the tip over the insulating substrate. It can be seen that the intensity decays more rapidly with distance to the left than with an equal distance to the right, indicating that transport of the analyte on the dark side of the array can be discerned from the diffusion of the fluorescent product alone. Diffusion of resorufin will of course lead to a decrease in spatial resolution at extended experiment times. This can possibly be hindered or even completely prevented by immobilizing these fluorescent molecules on the surface of the bipolar electrodes. However this may significantly decrease our upper limit of detection by lowering the concentration of fluorogenic reaction precursor available at or near the electrode surface. We are currently investigating methods to immobilize resazurin onto the electrodes without adversely affecting our detection limit.

To further explore the spatial resolution provided by FEEM in its present setting, a carbon-fiber array was patterned with photoresist on the anodic side (top) to physically block the oxidation of FcMeOH on selected regions of the bipolar electrode array. Only the carbon fiber surfaces inside the Husky pattern, shown in Figure SI5a, are exposed to FcMeOH solution, while the rest of the areas are covered with photoresist. No photoresist was placed on the cathodic side of the array where the fluorescence was observed. The FEEM image shown in Figure SI5b provides a clear representation of the oxidation of 2 mM FcMeOH at the anodic poles of the

dx.doi.org/10.1021/ja310401b | J. Am. Chem. Soc. 2013, 135, 855−861

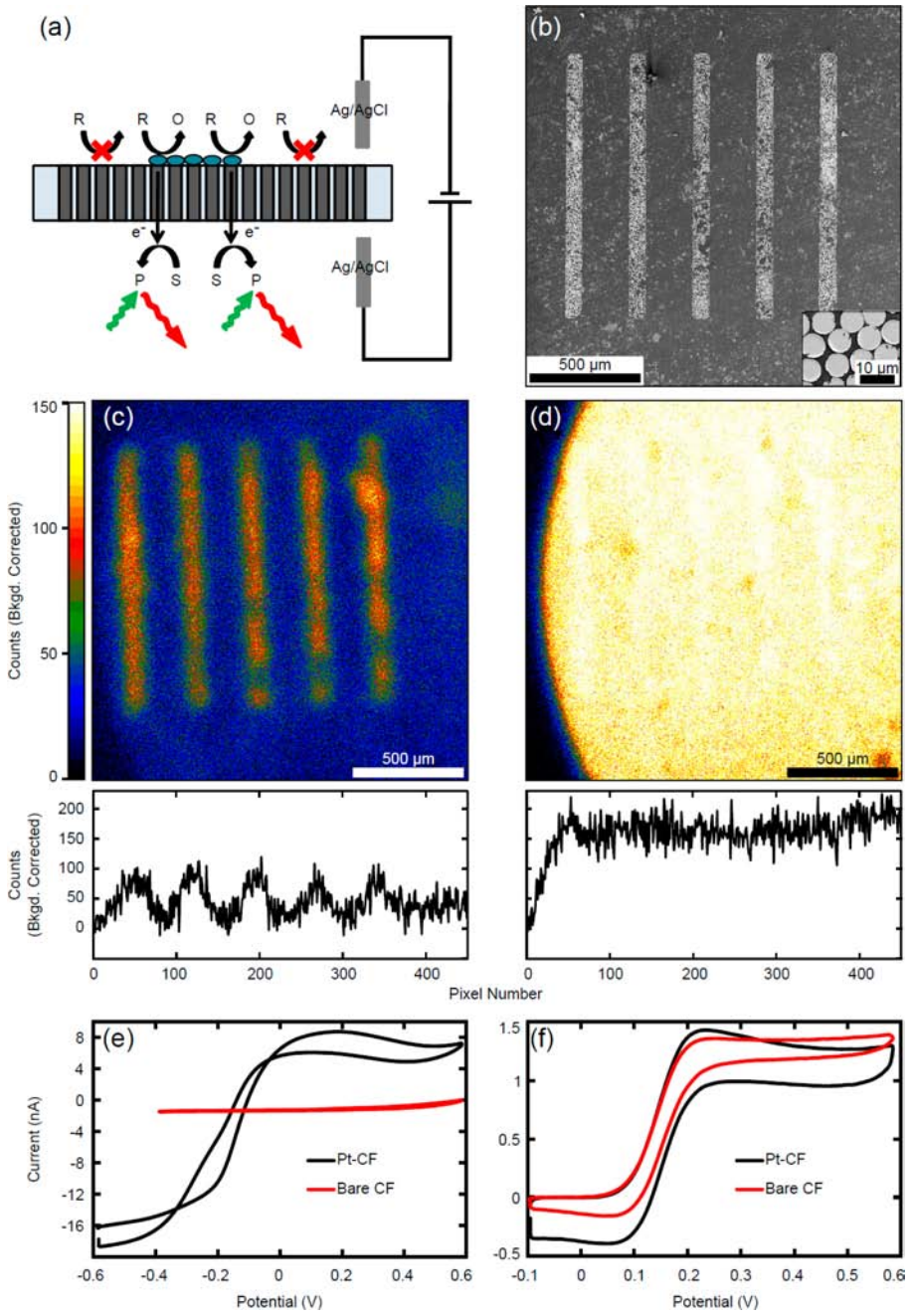

Figure 5. (a) Schematic showing the experimental design. (b) SEM image showing the pattern of Pt deposition on the CF array surface with an inset showing a region of Pt deposition. (c) FEEM image (top) and line scan (bottom) showing the oxidation of 10 mM H_2O_2 in 0.1 M NaOH at catalytically active "hot-spots" where Pt was deposited on a CF array. (d) FEEM image for the same Pt patterned CF array showing the nonselective oxidation of 2 mM FcMeOH in 0.1 M KCl. (e,f) Cyclic voltammetric response of a single 5 μm diameter CF electrode in 10 mM H_2O_2 and 2 mM FcMeOH, respectively, before and after Pt deposition on the electrode surface.

array, and the pattern is well resolved. There are however noticeable distortions to the image seen in Figure SI5b as compared to the pattern in Figure SI5a. For example, in the fluorescent signal we see a brighter section at the jaw line of the Husky, flanked by two less intense regions. This distortion is likely due to irregularities in the original carbon fiber array, such as lateral crosstalk or convergence/divergence of adjacent wires. We have found that very thin cross sections of the array, as thin as 100 μm, greatly reduce image distortions. We are working to incorporate highly ordered nanowire arrays into our setup to virtually eliminate this issue. The resolution of FEEM is currently limited by the size of each of the individual carbon fibers of the array, ~6 μm for the arrays used here. However, we anticipate greatly increasing the spatial resolution through the use of metallic nanowire arrays.

Electrochemical Imaging of Electrocatalytic Heterogeneity. Development of new electrocatalysts requires quick and rigorous screening to determine their activity. As a result, there has been an increasing demand for improved high-throughput screening methods. FEEM provides an excellent platform for quick, parallel screening of electrocatalytic materials. To demonstrate the use of FEEM for electrocatalyst screening, a simple experiment was carried out where a carbon fiber bipolar electrode array was selectively patterned with

dx.doi.org/10.1021/ja310401b | J. Am. Chem. Soc. 2013, 135, 855−861

platinum on one side and used to study the electrocatalytic oxidation of hydrogen peroxide (Figure 5a). SEM images of the array (Figure 5b) show the five regions where Pt ~200 nm thick was electrochemically deposited on individual carbon fibers within the array. The remaining bare carbon fibers were unmodified. A solution of 10 mM H_2O_2 in 0.1 M NaOH was placed on the dark side of the array with the Pt-coated carbon fibers (Pt-CF). A voltage ramp from −400 to 700 mV was applied on the bipolar array to allow for the oxidation of H_2O_2. A large contrast in the oxidation signal can be clearly seen between the Pt-covered region and the remaining bare fibers. Figure 5c shows an FEEM image (top) and corresponding line scan (bottom) taken at the peak fluorescence intensity from a video recorded during the potential sweep. The five regions corresponding to the Pt-CFs are well resolved in the fluorescence image showing the much higher electrocatalytic activity of Pt to H_2O_2 oxidation versus bare carbon fiber.

In a subsequent experiment the hydrogen peroxide solution was replaced with 2 mM FcMeOH in 0.1 M KCl, and the potential was swept from 0 to 1 V. Unlike H_2O_2, FcMeOH is oxidized by an outer-sphere mechanism, and therefore the electron transfer kinetics is relatively independent of the electrode material. This can be visualized using FEEM as shown in Figure 5d, where the entire array fluoresces almost uniformly. The voltammetric response of a single bare carbon fiber and resulting Pt-CF after deposition in the same solutions of H_2O_2 and FcMeOH are shown in Figure 5e,f, respectively. As expected the oxidation of hydrogen peroxide is strongly dependent upon the electrode material, showing a much greater current response after Pt deposition. The response of the bare CF and Pt-CF in FcMeOH, on the other hand, is very similar in magnitude. Slight differences in charging current and a more peak shaped response with the Pt-CF are likely due to increased surface roughness and an increased contribution due to linear diffusion.

The time derivative of the fluorescent signal intensity, like in the FEEM experiment using single electrodes shown in Figure 2, can be used to obtain information comparable to traditional electrochemical current signal. The fluorescent voltammetric response from the FEEM videos for the oxidation of H_2O_2 and FcMeOH is shown in Figure 6a,b, respectively. Like the conventional voltammetric response, the fluorescent voltammetric response shows a clear difference in the catalytic activity for a region of bare carbon fibers versus a region of Pt-CF with hydrogen peroxide oxidation but little difference in the response for FcMeOH oxidation. This simple demonstration of the possible application of FEEM to electrocatalyst screening uses only two materials, platinum and carbon fiber. However, large scale use of this method to interrogate an array containing hundreds of parallel, multicomponent materials could be realized with little additional cost or technical requirements. Furthermore, significant improvements to the resolution of FEEM can be expected through the use of highly uniform, dense electrochemical arrays.

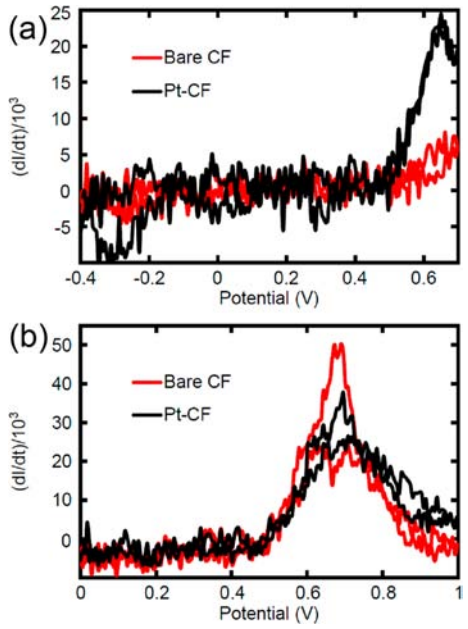

Figure 6. Time derivative of the fluorescence intensities for the experiment shown in Figure 5 as a function of potential for (a) the catalytic oxidation of 10 mM H_2O_2 at a Pt patterned CF array and (b) the oxidation of 2 mM FcMeOH in 0.1 M KCl at the same Pt patterned CF array.

CONCLUSIONS

In summary, we have studied the electrochemical coupling of a fluorogenic reduction reaction and conventional oxidation reactions (e.g., oxidation of Fc, dopamine, and H_2O_2) on closed bipolar microelectrodes and their array. The generation of a fluorescent product allows one to use highly sensitive fluorescence microscopy to observe electrochemical kinetics and monitor electrocatalytic heterogeneity over large electrochemical arrays. This is a unique electrochemical imaging approach to study many conventional electrochemical oxidation reactions with excellent spatial and temporal resolutions. We have shown the correlation between the derivative of fluorescence intensity and the electrochemical current and are currently carrying out additional studies in order to quantify this relationship. The use of fluorogenic oxidation reactions, such as the oxidation of cresyl violet or amplex red, may be used in future experiments to allow for the extension of this method to the detection of reducible analytes. We have briefly shown the applicability of FEEM to electrocatalyst screening and believe that it could serve as a useful platform for high-throughput, multicomponent, and parallel testing. The future incorporation of arrays of bipolar nanoelectrode into the FEEM configuration holds the possibility for reaching submicrometer or even diffraction-limited resolution.

ASSOCIATED CONTENT

Supporting Information

Derivation of the relationship between the Faradaic current on a closed bipolar electrode and the time derivative of the fluorescence intensity, SEM images of gold microelectrodes, a schematic diagram of the experimental setup for fluorescence-enabled electrochemical detection, SEM images of a carbon-fiber microelectrode array, fluorescence intensities for the data shown in Figure 4, and fluorescent image of the patterned Husky on a carbon-fiber array. This material is available free of charge via the Internet at http://pubs.acs.org.

AUTHOR INFORMATION

Corresponding Author

zhang@chem.washington.edu

Notes

The authors declare no competing financial interest.

■ ACKNOWLEDGMENTS

The authors gratefully acknowledge financial support from the National Science Foundation (CHE-1212805), and U.S. Defense Threat Reduction Agency (contract no. HDTRA1-11-1-0005). Part of this work was conducted at the University of Washington NanoTech User Facility, a member of the National Science Foundation, National Nanotechnology Infrastructure Network (NNIN). J.P.G. was supported by the American Chemical Society, Division of Analytical Chemistry Fellowship, sponsored by the Society of Analytical Chemists of Pittsburgh. B.Z. is the recipient of a Sloan Research Fellowship. The authors also thank Professor Charles T. Campbell for carefully reading the manuscript.

■ REFERENCES

(1) Sanchez-Sanchez, C. M.; Bard, A. J. *Anal. Chem.* **2009**, *81*, 8094−8100.
(2) Basame, S. B.; White, H. S. *Anal. Chem.* **1999**, *71*, 3166−3170.
(3) Kurulugama, R. T.; Wipf, D. O.; Takacs, S. A.; Pongmayteegul, S.; Garris, P. A.; Baur, J. E. *Anal. Chem.* **2005**, *77*, 1111−1117.
(4) Bard, A. J.; Fan, F. R. F.; Kwak, J.; Lev, O. *Anal. Chem.* **1989**, *61*, 131−138.
(5) Amemiya, S.; Bard, A. J.; Fan, F. -R. F.; Mirkin, M. V.; Unwin, P. R. *Annu. Rev. Anal. Chem.* **2008**, *1*, 95−131.
(6) Eckhard, K.; Chen, X.; Turcu, F.; Schuhmann, W. *Phys. Chem. Chem. Phys.* **2006**, *8*, 5359−5365.
(7) Fernandez, J. L.; Walsh, D. A.; Bard, A. J. *J. Am. Chem. Soc.* **2005**, *127*, 357−365.
(8) Scott, E. R.; White, H. S.; Phipps, J. B. *Anal. Chem.* **1993**, *65*, 1537−1545.
(9) McKelvey, K.; Snowden, M. E.; Peruffo, M.; Unwin, P. R. *Anal. Chem.* **2011**, *83*, 6447−6454.
(10) Uitto, O. D.; White, H. S. *Anal. Chem.* **2001**, *73*, 533−539.
(11) Shen, M.; Ishimatsu, R.; Kim, J.; Amemiya, S. *J. Am. Chem. Soc.* **2012**, *134*, 9856−9859.
(12) Bard, A. J.; Li, X.; Zhan, W. *Biosens. Bioelectron.* **2006**, *22*, 461−472.
(13) Schulte, A.; Nebel, M.; Schuhmann, W. *Annu. Rev. Anal.Chem.* **2010**, *3*, 299−318.
(14) Gardner, C. E.; Macpherson, J. V. *Anal. Chem.* **2002**, *74*, 576A−584A.
(15) Morris, C. A.; Friedman, A. K.; Baker, L. A. *Analyst* **2010**, *135*, 2190−2202.
(16) Comstock, D. J.; Elam, J. W.; Pellin, M. J.; Hersam, M. C. *Anal. Chem.* **2010**, *82*, 1270−1276.
(17) Takahashi, Y.; Shevchuk, A. I.; Novak, P.; Murakami, Y.; Shiku, H.; Korchev, Y. E.; Matsue, T. *J. Am. Chem. Soc.* **2010**, *132*, 10118−10126.
(18) Cortes-Salazar, F.; Momotenko, D.; Lesch, A.; Wittstock, G.; Girault, H. H. *Anal. Chem.* **2010**, *82*, 10037−10044.
(19) Lescha, A.; Momotenkob, D.; Cortés-Salazarb, F.; Wirthc, I.; Tefashea, U. M.; Meinersa, F.; Vaskea, F.; Giraultb, H. H.; Wittstock., G. *J. Electroanal. Chem.* **2012**, *666*, 52−61.
(20) Shan, X.; Patel, U.; Wang, S.; Iglesias, R.; Tao, N. J. *Science* **2010**, *327*, 1363−1366.
(21) Shan, X.; Díez-Pérez, I.; Wang, L.; Wiktor, P.; Gu, Y.; Zhang, L.; Wang, W.; Lu, J.; Wang, S.; Gong, Q.; Li, J. H.; Tao, N. J. *Nat. Nanotechnol.* **2012**, *7*, 668−672.
(22) Foley, K. J.; Shan, X.; Tao, N. J. *Anal. Chem.* **2008**, *80*, 5146−5151.
(23) Wang, W.; Foley, K.; Shan, X.; Wang, S.; Eaton, S.; Nagaraj, V. J.; Wiktor, P.; Patel, U.; Tao, N. J. *Nat. Chem.* **2011**, *3*, 249−253.
(24) Shan, X.; Wang, S.; Wang, W.; Tao, N. *Anal. Chem.* **2011**, *83*, 7394−7399.
(25) Zhang, B.; Adams, K. L.; Luber, S. J.; Eves, S. J.; Heien, M. L.; Ewing, A. G. *Anal. Chem.* **2008**, *80*, 1394−1400.
(26) Zhang, B.; Heien, M. L. A. V.; Santillo, M. F.; Mellander, L.; Ewing, A. G. *Anal. Chem.* **2011**, *83*, 571−577.
(27) Lin, Y.; Trouillon, R.; Svensson, M. I.; Keighron, J. D.; Cans, A.-S.; Ewing, A. G. *Anal. Chem.* **2012**, *84*, 2949−2954.
(28) Mavre, F.; Anand, R. K.; Laws, D. R.; Chow, K. F.; Chang, B. Y.; Crooks, J. A.; Crooks, R. M. *Anal. Chem.* **2010**, *82*, 8766−8774.
(29) Guerrette, J. P.; Oja, S. M.; Zhang, B. *Anal. Chem.* **2012**, *84*, 1609−1616.
(30) Gesquiere, A. J.; Park, S. J.; Barbara, P. F. *J. Phys. Chem. B* **2004**, *108*, 10301−10308.
(31) Palacios, R. E.; Fan, F.-R. F.; Bard, A. J.; Barbara, P. F. *J. Am. Chem. Soc.* **2006**, *128*, 9028−9029.
(32) Palacios, R. E.; Fan, F.-R. F.; Grey, J. K.; Suk, J.; Bard, A. J.; Barbara, P. F. *Nat. Mater.* **2007**, *6*, 680−685.
(33) Lei, C.; Hu, D.; Ackerman, E. J. *Chem. Commun.* **2008**, 5490−5492.
(34) Xu, W.; Kong, J. S.; Yeh, Y. T. E.; Chen, P. *Nat. Mater.* **2008**, *7*, 992−996.
(35) Xu, W.; Shen, H.; Kim, Y. J.; Zhou, X. C.; Liu, G. K.; Park, J.; Chen, P. *Nano Lett.* **2009**, *9*, 3968−3973.
(36) Smotkin, E. S.; Diaz-Morales, R. R. *Annu. Rev. Mater. Res.* **2003**, *33*, 557−579.
(37) Fosdick, S. E.; Crooks, R. M. *J. Am. Chem. Soc.* **2012**, *134*, 863−866.
(38) Han, K. S.; Liu, G. K.; Zhou, X. C.; Medina, R. E.; Chen, P. *Nano Lett.* **2012**, *12*, 1253−1259.
(39) Cox, J. T.; Guerrette, J. P.; Zhang, B. *Anal. Chem.* **2012**, *84*, 8797−8804.
(40) Adams, K. L.; Jena, B. K.; Percival, S. J.; Zhang, B. *Anal. Chem.* **2011**, *83*, 920−927.